Inorganic Chemistry

ARTICLE

pubs.acs.org/IC

1D + 1D → 1D Polyrotaxane, 2D + 2D → 3D Interpenetrated, and 3D Self-Penetrated Divalent Metal Terephthalate Bis(pyridylformyl)piperazine Coordination Polymers

Curtis Y. Wang,[†] Zachary M. Wilseck,[‡] and Robert L. LaDuca*[,‡]

[†]Diamond Bar High School, Diamond Bar, California 91765, United States

[‡]Lyman Briggs College and Department of Chemistry, E-30 Holmes Hall, Michigan State University, East Lansing, Michigan 48825, United States

Supporting Information

ABSTRACT: Divalent metal coordination polymers containing terephthalate (tere) and bis(4-pyridylformyl)piperazine (bpfp) show diverse and interesting two-dimensional (2D) interpenetrated, three-dimensional (3D) self-penetrated, or one-dimensional (1D) polyrotaxane topological features. Isostructural $\{[M(tere)(bpfp)(H_2O)_2]\bullet 4H_2O\}_n$ phases (**1**, Zn; **2**, Co) exhibit mutually inclined 2D + 2D → 3D interpenetration of gridlike layers. $\{[Cd_4(tere)_4(bpfp)_3(H_2O)_2]\cdot 8H_2O\}_n$ (**3**) possesses a novel 3,4,8-connected trinodal self-penetrated network with $(4.6^2)_2(4^26^{16}8^710^3)(4^26^4)_2$ topology. $[Zn_2Cl_2(tere)(bpfp)_2]_n$ (**4**) is the first example of a 1D + 1D → 1D polyrotaxane coordination polymer, to the best of our knowledge. Metal coordination geometry plays a crucial role in dictating the overall dimensionality in this system. Thermal decomposition behavior and luminescent properties of the d^{10} configuration metal derivatives are also presented herein.

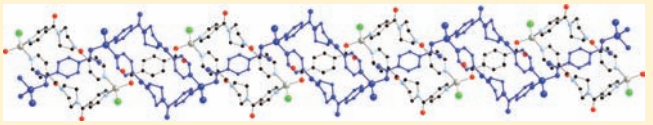

INTRODUCTION

Recent years have seen very heightened interest in the synthesis, structural characterization, and physical property measurements of crystalline coordination polymers, because of these solids' multifunctional applications in hydrogen storage,[1] selective molecular sorption,[2] ion exchange,[3] heterogeneous catalysis,[4] and nonlinear optics.[5] Aromatic dicarboxylate ligands have proven to be the most advantageous ligands for the self-assembly of coordination polymers, as they provide both structural scaffolding and necessary charge equalization.[6] Final preference for crystallization of a specific coordination polymer tends to rely on synergism between several competing factors, such as the geometric disposition of carboxylate groups and their ligating modes, metal-induced coordination geometry selectivity, and the occasional in situ formation of metal carboxylate cluster subunits. Specifically, the terephthalate (tere, 1,4-benzenedicarboxylate) ligand has proven useful in accessing three-dimensional (3-D) coordination polymer networks,[7−10] including the classic absorptive MOF-5 $[Zn_4O(tere)_3]_n$ phase reported by Yaghi,[7] and the giant hysteresis canted spin metamagnetic material $[Co_2(OH)_2(tere)]_n$ reported by Huang.[8] Functional properties or structural complexity in divalent metal terephthalate solids can be enhanced by the inclusion of nitrogen-base coligands. For example, the 2-fold interpenetrated 3-D phase $[Zn(tere)(4,4'\text{-bpy})_{0.5}]_n$ exhibits high carbon dioxide absorption selectivity.[9] The 3-D coordination polymer $[(CH_3)_2NH_2]_2$-$[Cd_5(tere)_4(1,2,4\text{-triazole})_2(benzotriazole)_2]_n$ is the unique example of a γ-Pu $3^{12}4^{26}5^7$ topology 10-connected net.[10]

Among the new numerous coordination polymer topologies uncovered in recent years, some of the most intriguing are self-penetrated lattices, wherein the shortest circuits within the network are penetrated by rods of the same network. These lattices can manifest elegant uninodal 3-connected and 4-connected networks, such as the 12^3 regular topology in a cationic $[Ni(tri\text{-}4\text{-}pyridyl\text{-}1,3,5\text{-}triazine)]_n^{2n+}$ framework[11] and the 7^48^2 topology in $\{[Cd(phthalate)(4,4'\text{-}dipyridylamine)(H_2O)]\cdot 3H_2O\}_n$,[12] respectively. Alternatively, self-penetrated coordination polymer networks may be more highly connected and complex, for example the $(4.8^2)(4.6^4.8^4.10)$ (3,5)-connected self-catenated binodal topology in $\{[Ni(oxybisbenzoate)(4,4'\text{-}bipyridine)]\cdot H_2O\}_n$[13] and an 8-connected $4^45^{17}6^7$ topology in $\{Co_3(oxybisbenzoate)_3(bpmp)_2]$ (bpmp = bis(4-pyridylmethyl)piperazine).[14] Although rare, some self-penetrated layered two-dimensional (2-D) nets have been seen, including $\{[Zn_3(OH)_3(dpp)_3](NO_3)_3\cdot 8.67H_2O\}_n$ (dpp = 1,3-bis(4-pyridyl)propane)[15] and $\{[Zn_3(tricarballylate)_2(bpmp)$-$(Hbpmp)_2](ClO_4)_2\cdot 5H_2O\}_n$,[16] which manifests threaded-loop polyrotaxane motifs.

A common trend in the design of many self-penetrated networks in metal−organic materials is the use of kinked and/or longer flexible tethering ligands, as these can promote helical or looped structural motifs through which other organic tethers can penetrate. Toward this aim we investigated the preparation of divalent metal terephthalate coordination polymers containing the long-spanning, conformationally flexible dipyridyl ligand bis(4-pyridylformyl)piperazine (bpfp).[17−21] This ligand has potential multitopic binding ability at its pyridyl rings and its formyl groups; it can adopt either trans or cis conformations

Received: June 8, 2011
Published: July 21, 2011

Scheme 1. Conformations of Bis(4-pyridylformyl)piperazine (bpfp)

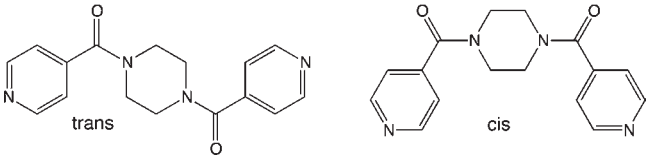

(Scheme 1), in response to local supramolecular conditions during coordination polymer self-assembly. A pair of cis conformation bpfp ligands linking a pair of metal ions, as seen in the layered copper nitrate phase $\{[Cu(bpfp)_2(NO_3)](NO_3)\cdot 8H_2O\}_n$,[18] could permit a large enough aperture into which a rigid-rod terephthalate ligand could penetrate. In this contribution we present the synthesis, structural characterization, and luminescent and thermal properties of $\{[M(tere)(bpfp)(H_2O)_2]\cdot 4H_2O\}_n$ phases (**1**, Zn; **2**, Co), $\{[Cd_4(tere)_4(bpfp)_3(H_2O)_2]\cdot 8H_2O\}_n$ (**3**), and $[Zn_2Cl_2(tere)(bpfp)_2]_n$ (**4**). While **1** and **2** show a relatively common pattern of inclined interpenetrated coordination polymer grids, **3** manifests a unique, complicated self-penetrated network topology. To the best of our knowledge, compound **4** represents the first example of a parallel 1-D + 1-D → 1-D interpenetrated threaded-loop polyrotaxane coordination polymer. Luminescent properties and thermal decomposition behavior of these four new materials were also investigated.

EXPERIMENTAL SECTION

General Considerations. Metal salts were purchased from Aldrich. Potassium terephthalate was prepared by the deprotonation of terephthalic acid with potassium hydroxide. Bis(4-pyridylformyl)piperazine (bpfp) was prepared using a published procedure.[17] Water was deionized above 3 MΩ cm in-house. IR spectra were recorded on powdered samples using a Perkin-Elmer Spectrum One instrument. The luminescence spectra were obtained with a Hitachi F-4500 fluorescence spectrometer on solid crystalline samples anchored to quartz microscope slides with Rexon Corporation RX-22P ultraviolet-transparent epoxy adhesive. Thermogravimetric analysis was performed on a TA Instruments high-resolution Q500 thermal analyzer under flowing N_2.

Preparation of $[Zn(tere)(bpfp)(H_2O)_2]\cdot 4H_2O\}_n$ (1). $Zn(ClO_4)_2\cdot 6H_2O$ (138 mg, 0.37 mmol), bpfp (109 mg, 0.37 mmol), potassium terephthalate (89 mg, 0.37 mmol), and 10 mL of deionized water were placed into a 23 mL acid digestion bomb. The bomb was sealed and heated in an oil bath at 150 °C for 48 h, and then cooled slowly to 25 °C. Colorless blocks of **1** (142 mg, 60% yield based on Zn) were isolated after washing with distilled water, ethanol, and acetone and drying in air. Anal. Calcd for $C_{24}H_{32}N_4O_{12}Zn$ **1**: C, 45.47; H, 5.09; N, 8.84%. Found: C, 45.08; H, 4.87; N, 8.45%. IR (cm^{-1}): 3569 (w), 3419 (w), 3043 (w), 2926 (w), 1714 (w), 1606 (s), 1540 (s), 1503 (w), 1472 (w), 1444 (w), 1416 (w), 1377 (s), 1362 (s), 1285 (s), 1265 (s), 1218 (w), 1163 (w), 1095 (w), 1069 (w), 1054 (w), 1009 (s), 968 (w), 922 (w), 906 (w), 890 (w), 840 (s), 794 (s), 751 (s), 715 (s), 682 (w).

Preparation of $[Co(tere)(bpfp)(H_2O)_2]\cdot 4H_2O\}_n$ (2). $CoCl_2\cdot 6H_2O$ (88 mg, 0.37 mmol), bpfp (109 mg, 0.367 mmol), potassium terephthalate (89 mg, 0.37 mmol), and 10 mL of deionized water were placed into a 23 mL acid digestion bomb. The bomb was sealed and heated in an oil bath at 120 °C for 48 h, and then cooled slowly to 25 °C. Pink needles of **2** (75 mg, 32% yield based on Co) were isolated after washing with distilled water, ethanol, and acetone and drying in air. Anal. Calcd for $C_{24}H_{32}CoN_4O_{12}$ **2**: C, 45.94; H, 5.14; N, 8.93%. Found: C, 46.01; H, 4.83; N, 8.90%. IR (cm^{-1}): 3575 (w), 3418 (w), 2871 (w), 1607 (s), 1541 (s), 1504 (w), 1472 (w), 1444 (w), 1416 (w), 1379 (s), 1363 (w), 1286 (s), 1266 (s), 1218 (w), 1164 (w), 1113 (w), 1096 (w), 1070 (w), 1055 (w), 1010 (s), 969 (w), 929 (w), 907 (w), 892 (w), 839 (s), 795 (s), 754 (s), 743 (w), 716 (w).

Preparation of $\{[Cd_4(tere)_4(bpfp)_3(H_2O)_2]\cdot 8H_2O\}_n$ (3). $Cd(NO_3)_2\cdot 4H_2O$ (114 mg, 0.37 mmol), potassium terephthalate (89 mg, 0.37 mmol), and bpfp (109 mg, 0.37 mmol) were placed into 10 mL of distilled H_2O in a 23 mL Teflon-lined Parr acid digestion bomb. The bomb was sealed and heated at 120 °C for 48 h, whereupon it was cooled slowly to 25 °C. Colorless blocks of **3** (62 mg, 31% yield based on Cd) were isolated after washing with distilled water and acetone and drying in air. Anal. Calcd for $C_{80}H_{84}Cd_4N_{12}O_{32}$ **3**: C, 44.17; H, 3.89; N, 7.73%. Found: C, 44.03; H, 3.60; N, 8.38%. IR (cm^{-1}): 3333 (w), 3048 (w), 2911 (w), 1632 (m), 1612 (w), 1593 (w), 1551 (s), 1504 (w), 1453 (w), 1438 (w), 1418 (w), 1381 (s), 1266 (s), 1220 (w), 1159 (w), 1103 (w), 1069 (w), 1044 (w), 1001 (s), 887 (w), 835 (s), 749 (s), 712 (w), 653 (w).

Preparation of $[Zn_2Cl_2(tere)(bpfp)_2]_n$ (4). $ZnCl_2$ (50 mg, 0.37 mmol), 4-bpfp (109 mg, 0.367 mmol), potassium terephthalate (89 mg, 0.37 mmol), and 10 mL of deionized water were placed into a 23 mL acid digestion bomb. The bomb was sealed and heated in an oil bath at 120 °C for 48 h, and then cooled slowly to 25 °C. Straw-colored needles of **4** (47 mg, 27% yield based on Zn) were isolated after washing with distilled water, ethanol, and acetone and drying in air. Anal. Calcd for $C_{40}H_{36}Cl_2N_8O_8Zn_2$ **4**: C, 50.13; H, 3.79; N, 11.69%. Found: C, 49.72; H, 3.41; N, 11.18%. IR (cm^{-1}): 3416 (w), 3097 (w), 2921 (w), 1977 (w), 1714 (w), 1621 (s), 1603 (s), 1548 (w), 1499 (w), 1461 (w), 1419 (s), 1386 (s), 1351 (s), 1283 (w), 1262 (s), 1220 (s), 1167 (w), 1142 (w), 1105 (w), 1087 (w), 1068 (w), 1029 (w), 1009 (s), 894 (w), 871 (w), 854 (w), 840 (w), 829 (s), 796 (w), 767 (w), 751 (s), 697 (s), 655 (s).

X-ray Crystallography. Single crystal X-ray diffraction data were collected for **1**−**4** using a Bruker-AXS ApexII CCD instrument at 173 K. Reflection data were acquired using graphite-monochromated Mo Kα radiation (λ = 0.710 73 Å). The data was integrated via SAINT.[22] Lorentz and polarization effect and empirical absorption corrections were applied with SADABS.[23] The structures were solved using direct methods and refined on F^2 using SHELXTL.[24] All non-hydrogen atoms were refined anisotropically. Hydrogen atoms bound to carbon atoms were placed in calculated positions and refined isotropically with a riding model. The hydrogen atoms bound to the unligated or ligated water molecules were found via Fourier difference maps where possible, and then restrained at fixed positions and refined isotropically. Relevant crystallographic data for **1**−**4** are listed in Table 1.

RESULTS AND DISCUSSION

Synthesis and Spectral Characterization. Compounds **1**−**4** were prepared as crystalline products by hydrothermal reaction of the appropriate metal salt, potassium terephthalate, and bpfp. The infrared spectra of **1**−**4** were consistent with their structural characteristics as determined by single-crystal X-ray diffraction. Weak and medium intensity bands in the range ∼1600 to ∼1200 cm^{-1} can be ascribed to stretching modes of the pyridyl rings of bpfp. Puckering modes of the pyridyl rings are evident in the region between 820 and 600 cm^{-1}. Asymmetric and symmetric C−O stretching modes of the carboxylate groups of fully deprotonated tere ligands correspond to the strong, broadened features at 1540 and 1377 cm^{-1} (for **1**), 1541 and 1379 cm^{-1} (for **2**), 1551 and 1381 cm^{-1} (for **3**), and 1603 and 1419 cm^{-1} (for **4**). Broad yet weak bands in the region ∼3400 to ∼3200 cm^{-1} represent O−H bonds within ligated and/or unbound water molecules in **1**−**3**. The broadness of

dx.doi.org/10.1021/ic201196g |Inorg. Chem. 2011, 50, 8997–9003

Table 1. Crystal and Structure Refinement Data for 1−4

	1	2	3	4
empirical formula	$C_{24}H_{32}N_4O_{12}Zn$	$C_{24}H_{32}CoN_4O_{12}$	$C_{80}H_{84}Cd_4N_{12}O_{32}$	$C_{40}H_{36}Cl_2N_8O_8Zn_2$
fw	633.91	625.45	2175.19	958.41
cryst syst	monoclinic	monoclinic	triclinic	monoclinic
space group	$P2_1/c$	$P2_1/c$	$P\bar{1}$	$P2_1/c$
a (Å)	11.114(3)	11.120(3)	9.5104(13)	10.4159(8)
b (Å)	11.991(3)	12.006(3)	12.7291(17)	18.6675(15)
c (Å)	11.422(3)	11.406(3)	19.131(3)	10.0697(8)
α (deg)	90	90	100.348(2)	90
β (deg)	119.110(1)	119.161(3)	97.090(1)	98.734(1)
γ (deg)	90	90	107.716(1)	90
V (Å^3)	1329.8(6)	1329.9(6)	2130.7(5)	1935.2(3)
Z	2	2	1	2
D_{calcd} (g cm^{-3})	1.583	1.562	1.695	1.645
μ (mm^{-1})	0.996	0.718	1.078	1.444
hkl ranges	$-13 \le h \le 1$w	$-13 \le h \le 11$	$-11 \le h \le 11$	$-12 \le h \le 12$
	$-14 \le k \le 14$	$0 \le k \le 14$	$-15 \le k \le 14$	$-22 \le k \le 22$
	$-13 \le l \le 13$	$0 \le l \le 13$	$0 \le l \le 22$	$-12 \le l \le 12$
total reflns	9565	29 405	29 954	14 019
unique reflns	2441	2403	7488	3507
R(int)	0.0257	0.0982	0.0455	0.0666
params/restraints	205/9	199/6	601/15	271/0
R1[a] (all data)	0.0347	0.0760	0.0488	0.0637
R1 ($I > 2\sigma(I)$)	0.0299	0.0597	0.0323	0.0401
wR2[b] (all data)	0.0942	0.1516	0.0714	0.0882
wR2 ($I > 2\sigma(I)$)	0.0902	0.1431	0.0689	0.0787
max/min residual (e$^-$/Å^3)	0.285/−0.724	0.485/−0.998	1.244/−0.783	0.406/−0.342
GOF	1.080	1.114	0.853	1.032

[a] $R1 = \Sigma||F_o| - |F_c||/\Sigma|F_o|$. [b] $wR2 = \{\Sigma[w(F_o^2 - F_c^2)^2]/\Sigma[wF_o^2]^2\}^{1/2}$.

these higher energy spectral features is caused by hydrogen bonding interactions (see below). The presence of the bpfp formyl groups within **1**−**4** is indicated by strong C═O stretching bands between ∼1600 and ∼1630 cm^{-1}.

*Structural Description of [M(tere)(bpfp)(H$_2$O)$_2$]·4H$_2$O}$_n$ (**1**, Zn; **2**, Co).* As both compounds **1** and **2** are isostructural, only the structural features of **1** will be discussed in detail. The asymmetric unit of **1** contains a divalent zinc atom on a crystallographic inversion center, one-half of a terephthalate dianion, one-half of a trans conformation bpfp ligand, an aqua ligand, and two water molecules of crystallization. Operation of the inversion center at cobalt reveals a $\{ZnN_2O_4\}$ coordination sphere, with two bpfp pyridyl donors, two aqua ligands, and two tere carboxylate oxygen donors. Bond lengths and angles within the coordination environments for **1** and **2** obey well-known radius trends,[25] and are listed in Table 2.

Bis(monodentate) tere ligands connect zinc atoms into linear $[Zn(H_2O)_2(tere)]_n$ chains, with a metal−metal through-ligand contact distance of 11.422 Å. Hydrogen bonding donation from aqua ligands to unligated tere carboxylate oxygen atoms (O···O distance = 2.640(2) Å) provides some additional stabilization. In turn, $[Zn(H_2O)_2(tere)]_n$ chains are connected into $[Zn(H_2O)_2(tere)(bpfp)]_n$ (4,4) grid layers (Figure 1a) by dipodal trans conformation bpfp ligands, which span a Zn···Zn internuclear distance of 16.35 Å. The through-space apertures within a single layer submotif measure 16.56 × 22.83 Å, with Zn···Zn···Zn angles of 70.7° and 109.3°. The large rectangular windows within the layers permit mutual inclined interpenetration of parallel sets of layers (Figure 1b), at an angle of 78.0° as determined by TOPOS.[26] The comparable interpenetration angle for **2** is 77.9°. Hydrogen bonding between aqua ligands in one layer and bpfp formyl oxygen atoms in another (O···O distance = 2.899(2) Å) serves to stabilize the system of interpenetrated layers. Water molecule pairs in **1** lie in small solvent-accessible voids, totaling 15.8% of the

Table 2. Selected Bond Distances (Å) and Angles (deg) Data for 1 and 2[a]

Zn1−O4	2.0743(16)	Co1−O4	2.055(2)
Zn1−O1	2.1364(15)	Co1−O1	2.113(3)
Zn1−N1	2.1677(17)	Co1−N1	2.158(3)
O4−Zn1−O4$^{\#1}$	180.0	O4$^{\#2}$−Co1−O4	180.0
O4−Zn1−O1	89.76(6)	O4$^{\#2}$−Co1−O1	89.96(11)
O4$^{\#1}$−Zn1−O1	90.24(6)	O4−Co1−O1	90.04(11)
O1$^{\#1}$−Zn1−O1	180.0	O1$^{\#2}$−Co1−O1	180.00(13)
O4−Zn1−N1	89.92(6)	O4$^{\#2}$−Co1−N1	89.79(11)
O4$^{\#1}$−Zn1−N1	90.08(6)	O4−Co1−N1	90.21(11)
O1$^{\#1}$−Zn1−N1	93.67(7)	O1$^{\#2}$−Co1−N1	93.83(12)
O1−Zn1−N1	86.33(7)	O1−Co1−N1	86.17(12)
N1$^{\#1}$−Zn1−N1	180.0	N1$^{\#2}$−Co1−N1	180.0

[a] Symmetry transformations to generate equivalent atoms: #1 $-x, -y, -z$; #2 $-x+1, -y, -z+1$.

dx.doi.org/10.1021/ic201196g |*Inorg. Chem.* 2011, 50, 8997–9003

overall unit cell volume (15.9° in **2**) as calculated by PLATON.[27] These are anchored in place by hydrogen bonding donation to unligated tere carboxylate groups and bpfp formyl groups.

Structural Description of $\{[Cd_4(tere)_4(bpfp)_3(H_2O)_2]\cdot 8H_2O\}_n$ (***3***). The asymmetric unit of compound **3** contains two divalent cadmium atoms (Cd1, Cd2), two tere ligands (tere-A, tere-B), one complete cis conformation bpfp ligand (bpfp-A), one-half of a trans conformation bpfp ligand (bpfp-B) whose piperazinyl ring centroid sits on a crystallographic inversion center, one aqua ligand, and four water molecules of crystallization. At Cd1 a distorted pentagonal bipyramidal $\{CdN_2O_5\}$ coordination environment is evident, with trans pyridyl nitrogen donor atoms from bpfp-A and bpfp-B in the axial positions. In the equatorial plane are located chelating carboxylate groups from one tere-A and one tere-B ligand, along with a single oxygen donor from a second tere-A ligand. A very distorted $\{CdO_5N\}$ octahedral coordination geometry exists at Cd2, with the equatorial sites filled by a chelating tere-B carboxylate group, a single oxygen donor from the monodentate terminus of tere-A, and a bpfp-B pyridyl nitrogen donor. A formyl oxygen from a bpfp-A ligand and an aqua ligand round out the coordination sphere at Cd2. Pertinent bond length and angle data for **3** are given in Table 3.

The crystallographically distinct tere ligands in **3** adopt different binding modes. The tere-A ligands connect to three cadmium atoms (two Cd1, one Cd2) with a μ_3-κ^3-O,O′:O′:O″ binding mode, while the tere-B ligands act as simple bis-(chelating) bridges between Cd1 and Cd2 atoms. Through the multidentate tere-A carboxylate groups, Cd1 atoms are connected into $\{Cd_2O_2\}$ dinuclear units with Cd···Cd and O···O distances of 3.987 and 2.991 Å, respectively. These connect to Cd2 atoms through the chelating termini of bridging tere-B ligands and tere-A monodentate carboxylate groups, to construct $[Cd_2(tere)_2(H_2O)]_n$ ribbon motifs that are oriented along the [101] crystal direction (Figure 2a).

Additionally, the cadmium atoms and bpfp ligands in **3** construct $[Cd_4(bpfp)_3(H_2O)_2]_n$ coordination polymer layers (Figure 2b). These contain chains of Cd1-based $\{Cd_2O_2\}$ dinuclear units and Cd2 atoms linked by cis conformation exotridentate μ_3-κ^3-N:N′:O bpfp-A ligands (O−C···C−O torsion angle = 2.8°), connected into two dimensions by trans conformation bridging bpfp-B ligands ligands (O−C···C−O torsion angle = 180°). These layer submotifs connect $[Cd_2(tere)_2(H_2O)]_n$ ribbons into a complex 3-D $[Cd_4(tere)_4(bpfp)_3(H_2O)_2]_n$ coordination polymer network (Figure 3). Water molecule pairs occupy small solvent-accessible voids (8.8% of the unit cell volume) within the framework of **3**.

In order to understand the underlying topology of the complex 3-D network of **3** more fully, a "node and linker" approach was undertaken. In this treatment, the exotridentate bpfp-A ligands, Cd2 atoms and $\{Cd_2O_2\}$ dinuclear units constructed from Cd1 atoms are considered 3-connected, 4-connected, and 8-connected nodes, respectively. The bpfp-A nodes connect to one $\{Cd_2O_2\}$ dinuclear unit and one Cd2 atom through its pyridyl groups, and to a second Cd2 atom through its lone formyl group donor. The Cd2 atoms are linked to two different bpfp-A nodes (via pyridyl and formyl donors), and to two $\{Cd_2O_2\}$ dinuclear units through tere ligands. The high connectivity $\{Cd_2O_2\}$ dinuclear nodes connect to two bpfp-A nodes via pyridyl ligation, two other $\{Cd_2O_2\}$ nodes through bpfp-B linkers, and four Cd2 nodes through tere ligands. The resulting 3,4,8-connected trinodal network (Figure 4) has a Schläfli symbol of $(4.6^2)_2$-$(4^26^4)_2(4^26^{16}8^710^3)$ as calculated by TOPOS. Moreover, the shortest 4-membered circuits engage in self-penetration into the shortest 6-membered circuits (Figure 5). A full topological analysis of the self-penetrated net of **3** is given in the Supporting Information. High nodal connectivity has been seen previously as means of promoting the formation of rare self-penetrated nets, for example in the 8-connected **ilc** $4^{24}5.6^3$ topology nets in $[Zn_5(\mu_3\text{-}OH)_2(terephthalate)_4(1,10\text{-}phenanthroline)_2]_n$[28] and $\{[Cu_4(1,4\text{-}phenylenediacetate)_3(OH)_2(dpp)_2]\cdot 2H_2O\}_n$,[29] along with the 8-connected $4^45^{17}6^7$ topology net in $[Co_3(oxybis\text{-}benzoate)_3(bpmp)_2]_n$.[14]

Structural Description of $[Zn_2Cl_2(tere)(bpfp)_2]_n$ (***4***). The asymmetric unit of compound **4** contains a divalent zinc atom, a chloro ligand, a full bpfp ligand, and one-half of a tere ligand whose phenyl ring centroid sits on a crystallographic inversion center. In contrast to **1**, there is a lack of aqua ligands, inducing a distorted $\{ZnN_2OCl\}$ tetrahedral coordination environment.

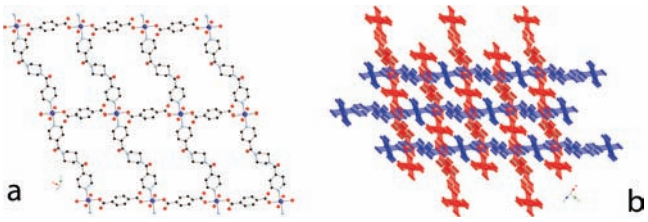

Figure 1. (a) Single $[Zn(H_2O)_2(tere)(bpfp)]_n$ (4,4) layer in **1**. (b) Mutual interpenetration of parallel sets of layers in **1**.

Table 3. Selected Bond Distances (Å) and Angles (deg) data for 3[a]

Cd1−N3	2.298(3)	O12−Cd1−O9	137.55(10)
Cd1−N5	2.300(3)	O5−Cd1−O9	53.36(9)
Cd1−O12	2.307(2)	$O11^{\#1}$−Cd1−O9	95.93(9)
Cd1−O5	2.327(3)	N3−Cd1−O11	89.14(10)
$Cd1-O11^{\#1}$	2.350(3)	N5−Cd1−O11	97.69(10)
Cd1−O9	2.558(3)	O12−Cd1−O11	52.65(9)
Cd1−O11	2.626(3)	O5−Cd1−O11	136.96(9)
Cd2−O8	2.219(3)	$O11^{\#1}$−Cd1−O11	73.65(9)
Cd2−O3	2.275(3)	O9−Cd1−O11	169.56(9)
$Cd2-N4^{\#2}$	2.317(3)	O8−Cd2−O3	84.85(12)
$Cd2-O10^{\#3}$	2.363(3)	$O8-Cd2-N4^{\#2}$	135.73(12)
$Cd2-O6^{\#3}$	2.384(3)	$O3-Cd2-N4^{\#2}$	94.10(12)
$Cd2-O7^{\#4}$	2.449(3)	$O8-Cd2-O10^{\#3}$	135.49(11)
N3−Cd1−N5	168.36(11)	$O3-Cd2-O10^{\#3}$	108.96(13)
N3−Cd1−O12	102.12(10)	$N4^{\#2}-Cd2-O10^{\#3}$	86.64(11)
N5−Cd1−O12	89.51(10)	$O8-Cd2-O6^{\#3}$	80.26(10)
N3−Cd1−O5	87.38(11)	$O3-Cd2-O6^{\#3}$	113.44(12)
N5−Cd1−O5	93.92(11)	$N4^{\#2}-Cd2-O6^{\#3}$	137.92(10)
O12−Cd1−O5	86.33(10)	$O10^{\#3}-Cd2-O6^{\#3}$	55.29(10)
$N3-Cd1-O11^{\#1}$	88.61(11)	$O8-Cd2-O7^{\#4}$	91.21(11)
$N5-Cd1-O11^{\#1}$	84.32(11)	$O3-Cd2-O7^{\#4}$	164.96(14)
$O12-Cd1-O11^{\#1}$	124.52(9)	$N4^{\#2}-Cd2-O7^{\#4}$	78.61(11)
$O5-Cd1-O11^{\#1}$	149.00(9)	$O10^{\#3}-Cd2-O7^{\#4}$	83.96(11)
N3−Cd1−O9	89.99(10)	$O6^{\#3}-Cd2-O7^{\#4}$	80.03(11)
N5−Cd1−O9	81.58(10)		

[a] Symmetry transformations to generate equivalent atoms: #1 $-x+2$, $-y+2$, $-z+1$; #2 $x-1$, y, $z+1$; #3 $x+1$, y, $z+1$; #4 $-x+2$, $-y+1$, $-z+1$.

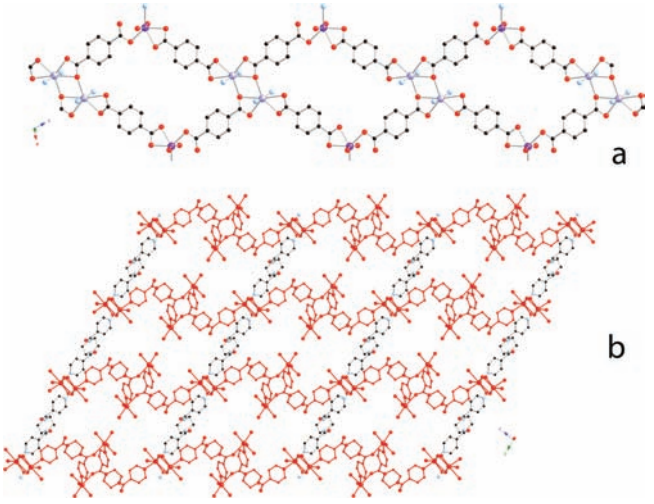

Figure 2. Submotifs in **3**. (a) $[Cd_2(tere)_2(H_2O)]_n$ ribbon. Cd1 and Cd2 atoms are shown in light and dark purple, respectively. (b) $[Cd_4(bpfp)_3(H_2O)_2]_n$ layer. The cis conformation bpfp ligands are drawn in red.

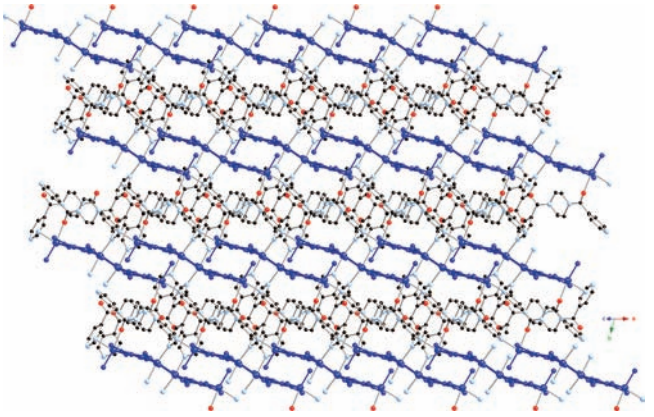

Figure 3. Complex $[Cd_4(tere)_4(bpfp)_3(H_2O)_2]_n$ coordination polymer 3-D net in **3**. $[Cd_2(tere)_2(H_2O)]_n$ ribbon motifs are depicted in dark blue.

Bond lengths and angles within the coordination environment of **4** are given in Table 4.

Operation of the crystallographic symmetry reveals the presence of $[Zn_2Cl_2(bpfp)_2]$ rings, where the zinc atoms are bridged by pairs of twisted cis conformation bpfp tethers, with a 59.7° O−C···C−O dihedral angle between formyl groups on the same ligand. Within the bpfp ligands, the piperazinyl rings adopt a "boat" conformation, heretofore unseen in any bpfp-containing coordination complexes. Adjacent $[Zn_2Cl_2(bpfp)_2]$ rings are connected into 1-D $[Zn_2Cl_2(tere)(bpfp)_2]_n$ coordination polymer chains (Figure 6a) along the *c* crystal axis by means of bis(monodentate) tere ligands; these span a Zn···Zn contact distance of 11.035 Å.

The Zn···Zn through-space distances across the 30-membered $[Zn_2Cl_2(bpfp)_2]$ rings within the $[Zn_2Cl_2(tere)(bpfp)_2]_n$ chains measure 13.304 Å. These circuits are large enough to permit the tere ligands of a second $[Zn_2Cl_2(tere)(bpfp)_2]_n$ chain to penetrate through the entire length of the first chain in a parallel manner (Figure 6b). The resulting 1D + 1D → 1D polyrotaxane coordination polymer entanglement is unprecedented

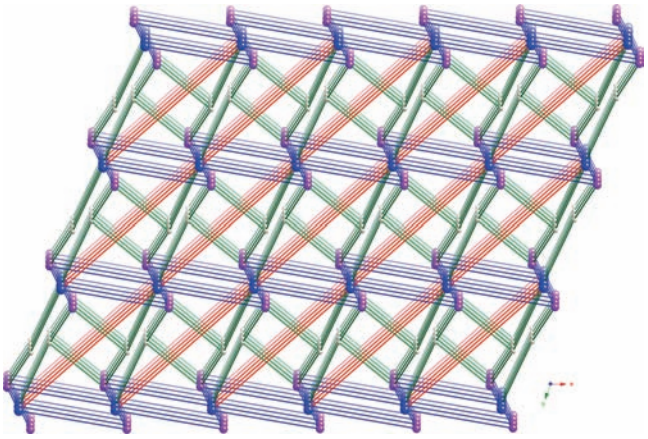

Figure 4. Schematic perspective of the unique self-penetrated 3,4,8-connected trinodal network of **3**. Gray, blue, and violet spheres represent the 3-connected cis conformation bpfp-A nodes, Cd2 atom nodes, and Cd1-based $\{Cd_2O_2\}$ dinuclear units, respectively. Connections through tere, bpfp-A, and bpfp-B ligands are shown as blue, green, and red rods, respectively.

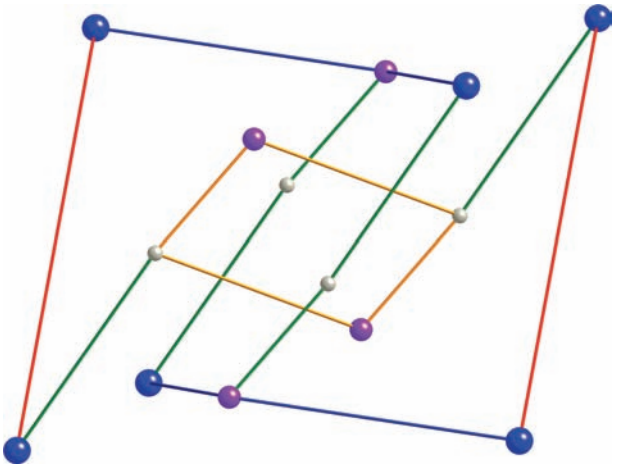

Figure 5. Close-up perspective of a self-penetration mechanism in **3**, whereby 4-membered circuits penetrate into the shortest 6-membered circuits.

to the best of our knowledge. However, precedent exists for similar polyrotaxane entanglement patterns in supramolecular aggregations of coordination complexes. In the organometallic cation $[\{(HO_2CC_6H_4CH_2)\text{-}(Bu_2bipy)Me_2Pt\}_3\{(tris(4\text{-pyridyl})triazine)\}]^{3+}$,[30] and in a solid state polymorph of 1,7-phenanthroline,[31] hydrogen-bonding interactions occur within open loops. In $[Zn_2(1\text{-bromo-}3,5\text{-bis(imidazol-1-ylmethyl)benzene})_2(OAc)_4]$,[32] Br···Br interactions between pendant halide groups cause the polyrotaxane motif. Parallel, neighboring 1D + 1D → 1D entangled chain pairs interact by nonclassical C−H···Cl interactions (C···Cl distance =3.383 Å) to construct the 3−D crystal structure of **4**.

THERMOGRAVIMETRIC ANALYSIS

For compound **1**, an 11.4% mass loss between 25 and 80 °C represented elimination of the water molecules of crystallization (11.2% loss calcd). Expulsion of the aqua ligands along with the

dx.doi.org/10.1021/ic201196g |*Inorg. Chem.* 2011, 50, 8997–9003

Table 4. Selected Bond Distances (Å) and Angle (deg) Data for 4[a]

Zn1−O1	1.944(2)
Zn1−N1$^{\#1}$	2.045(3)
Zn1−N4	2.065(3)
Zn1−Cl2	2.2341(10)
O1−Zn1−N1$^{\#1}$	119.42(10)
O1−Zn1−N4	116.69(10)
N1$^{\#1}$−Zn1−N4	100.90(11)
O1−Zn1−Cl2	106.28(8)
N1$^{\#1}$−Zn1−Cl2	108.25(8)
N4−Zn1−Cl2	104.17(8)

[a] Symmetry transformation to generate equivalent atoms: #1 $-x+1, -y, -z+3$.

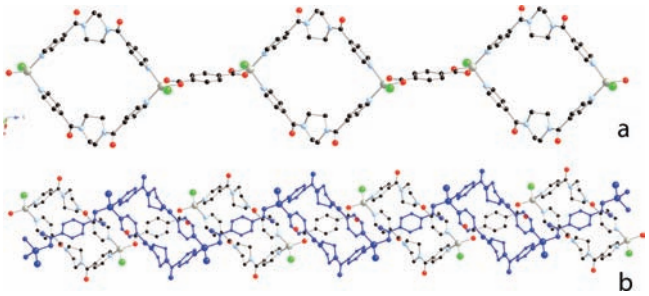

Figure 6. (a) $[Zn_2Cl_2(tere)(bpfp)_2]_n$ single chain in **4**. (b) Parallel 1D + 1D → 1D polyrotaxane entanglement of chain pairs in **4**.

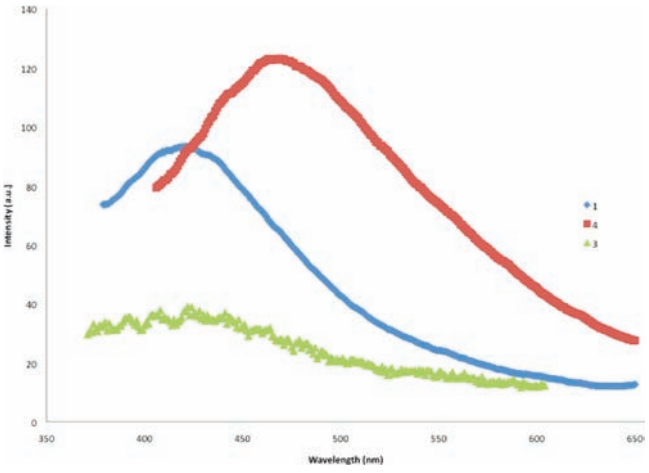

Figure 7. Luminescence spectra of **1**, **3**, and **4**.

dipyridyl and carboxylate ligands occurred above 250 °C, with the 21.1% mass remnant at 475 °C consistent with zinc carbonate (19.8% calcd). For compound **3**, dehydration occurred in several steps between 50 and 300 °C, as indicated by a total mass loss of 9.8% (8.3% calcd). Rapid elimination of the organic components occurred above 310 °C, with the final mass remnant at 475 °C roughly consistent with deposition of CdO (27.4% observed, 23.6% calcd). For compound **4**, the mass remained largely stable until 350 °C, at which temperature ligand pyrolysis ensued. The mass remnant of 41.8% at 475 °C indicates a possible deposition of zinc carbonate (26.2% calcd) and uncombusted organics. TGA traces for **1**, **3**, and **4** are given in Supporting Information Figures S1−S3, respectively.

Luminescent Properties of 1, 3, and 4. Irradiation of crystalline samples of the d^{10} configuration coordination polymers **1**, **3**, and **4** with ultraviolet light (λ_{ex} = 340 nm) resulted in moderately intense blue-violet visible light emission for the zinc-containing materials **1** and **4**, and very weak violet emission for the cadmium-containing phase **3** (Figure 7). Emission maxima for **1** and **4** were located at 420 and 465 nm, respectively, revealing a red shift upon reduction in coordination number from six to four. The weak emission of **3** was centered at 425 nm. The emissive behavior of these materials is attributed to $\pi-\pi^*$ or $\pi-n$ electronic transitions within the molecular orbitals of the aromatic rings of the tere and bpfp ligands.[33] It is plausible that the difference in binding mode of the tere ligands and in the conformation of the bpfp ligands of **3** results in a diminishing of emission intensity.

CONCLUSIONS

A dual structure directing effect of coordination geometry preference and conformation of bis(pyridylformyl)piperazine ligands appears to be active in this divalent metal terephthalate coordination polymer system. Octahedral coordination with trans-disposed, trans conformation bpfp ligands promotes formation of simple 2-D grid coordination polymers, with the long span of the bpfp ligand providing larger apertures and mutual inclined interpenetration. In the case of the larger cadmium ion, mixed pentagonal bipyramidal and octahedral coordination occurs. Via bpfp formyl group binding, accessing a cis ligand conformation, a complicated multinodal self-penetrated 3-D coordination polymer network was observed in **3**. Cis conformation bpfp pairs form loops in the tetrahedrally coordinated zinc-containing phase **4**, allowing penetration of rigid terephthalate rods within parallel coordination polymer chains. Thus, **4** is likely the first example of 1D + 1D → 1D polyrotaxane parallel coordination polymer chains. Combination of curled, looping dipyridyl ligands with shorter rigid rod dicarboxylates has proven a successful avenue for the generation of polyrotaxane-like coordination polymer structures.

ASSOCIATED CONTENT

Supporting Information. Additional figures and CIF data. This material is available free of charge via the Internet at http://pubs.acs.org. Topological analysis for **3**. Crystallographic data (excluding structure factors) for **1**−**4** have been deposited with the Cambridge Crystallographic Data Centre with Nos. 818809, 818808, 818807, and 818810, respectively. Copies of the data can be obtained free of charge via the Internet at http://www.ccdc.cam.ac.uk/conts/retrieving.html or by post at CCDC, 12 Union Road, Cambridge CB2 1EZ, U.K. (fax: 44-1223336033, email: deposit@ccdc.cam.ac.uk).

AUTHOR INFORMATION

Corresponding Author
*E-mail: laduca@msu.edu.

ACKNOWLEDGMENT

We acknowledge the donors of the American Chemical Society Petroleum Research Fund for funding this work. We

thank Dr. Stuart Batten of Monash University for very helpful discussions. C.W. thanks Dr. Gail Richmond and the Michigan State University High School Honors Science Program for participation in this research project.

REFERENCES

(1) (a) Murray, L. J.; Dinca, M.; Long, J. R. *Chem. Soc. Rev.* **2009**, *38*, 1294–1314 and references therein. (b) Han., S. S.; Mendoza-Cortes, J. L.; Goddard, W. A. *Chem. Soc. Rev.* **2009**, *38*, 1460–1476 and references therein.

(2) Li, J. R.; Kuppler, R. J.; Zhou, H. C. *Chem. Soc. Rev.* **2009**, *38*, 1477–1504 and references therein.

(3) (a) Plabst, M.; McCusker, L. B.; Bein, T. *J. Am. Chem. Soc.* **2009**, *131*, 18112–18118. (b) Liu, Y.; Kravtsov, V. C.; Eddaoudi, M. *Angew. Chem., Int. Ed.* **2008**, *47*, 8446–8449. (c) Nouar, F.; Eckert, J.; Eubank, J. F.; Forster, P.; Eddaoudi, M. *J. Am. Chem. Soc.* **2009**, *131*, 2864–2870.

(4) (a) Lee, J.; Farha, O. K.; Roberts, J.; Scheidt, K. A.; Nguyen, S. T.; Hupp, J. T. *Chem. Soc. Rev.* **2009**, *38*, 1450–1459 and references therein. (b) Ma, L.; Abney, C.; Lin, W. *Chem. Soc. Rev.* **2009**, *38*, 1248–1256 and references therein.

(5) Evans, O. R.; Lin, W. *Acc. Chem. Res.* **2002**, *35*, 511–522.

(6) Perry, J. J.; Perman, J. A.; Zaworotko, M. J. *Chem. Soc. Rev.* **2009**, *38*, 1400–1417 and references therein.

(7) Li, H.; Eddaoudi, M.; O'Keeffe, M.; Yaghi, O. M. *Nature* **1999**, *402*, 276–279.

(8) Huang, Z.; Drillon, M.; Masciocchi, N.; Sironi, A.; Zhao, J.; Rabu, P.; Panissod, P. *Chem. Mater.* **2000**, *12*, 2805–2812.

(9) Bastin, L.; Barcia, P. S.; Hurtado, E. J.; Silva, J. A. C.; Rodrigues, A. E.; Chen, B. *J. Phys. Chem. C* **2008**, *112*, 1575–1581.

(10) Wang, X.; Qin, C.; Lan, Y.; Shao, K.; Su, Z.; Wang, E. *Chem. Commun.* **2009**, 410–412.

(11) Abraham, B. F.; Batten, S. R.; Grannas, M. J.; Hamit, H.; Hoskins, B. F.; Robson, R. *Angew. Chem., Int. Ed.* **1999**, *38*, 1475–1477.

(12) Shyu, E.; Supkowski, R. M.; LaDuca, R. L. *Inorg. Chem.* **2009**, *48*, 2723–2725.

(13) Wang, X.-L.; Qin, C.; Wang, E.-B.; Su, Z.-M. *Chem.—Eur. J.* **2006**, *12*, 2680–2691.

(14) Martin, D. P.; LaDuca, R. L. *Inorg. Chem.* **2008**, *47*, 9754–9756.

(15) Plater, M. J.; Foreman, M. R.; Gelbrich, T.; Hursthouse, M. B. *J. Chem. Soc., Dalton Trans.* **2000**, 1995–2000.

(16) Farnum, G. A.; LaDuca, R. L. *Cryst. Growth Des.* **2010**, *10*, 1897–1903.

(17) Hou, H.; Song, Y.; Xu, H.; Wei, Y.; Fan, Y.; Zhu, Y.; Li, C.; Du, C. *Macromolecules* **2003**, *36*, 999–1008.

(18) Wilseck, Z. M.; LaDuca, R. L. *Inorg. Chem. Commun.* **2011**, *14*, 706–710.

(19) Wilseck, Z. M.; Gandolfo, C. M.; LaDuca, R. L. *Inorg. Chim. Acta* **2010**, *363*, 3865–3873.

(20) Wang, C. Y.; LaDuca, R. L. *J. Mol. Struct.* **2011**, *983*, 162–168.

(21) Wang, C. Y.; Wilseck, Z. M.; Supkowski, R. M.; LaDuca, R. L. *CrystEngComm* **2011**, *13*, 1391–1399.

(22) *SAINT, Software for Data Extraction and Reduction, Version 6.02*; Bruker AXS, Inc.: Madison, WI, 2002.

(23) *SADABS, Software for Empirical Absorption Correction. Version 2.03*; Bruker AXS, Inc.: Madison, WI, 2002.

(24) Sheldrick, G. M. *SHELXTL, Program for Crystal Structure Refinement*; University of Göttingen: Gottingen, Germany, 1997.

(25) Shannon, R. D. *Acta Crystallogr.* **1976**, *A32*, 751–767.

(26) Blatov, V. A.; Shevchenko, A. P.; Serezhkin, V. N. *J. Appl. Crystallogr.* **2000**, *33*, 1193. TOPOS software is available for download at http://www.topos.ssu.samara.ru.

(27) Spek, A. L. *PLATON, A Multipurpose Crystallographic Tool*; Utrecht University: Utrecht, The Netherlands, 1998.

(28) Wang, X. L.; Qin, C.; Wang, E. B.; Su, Z. M.; Xu, L.; Batten, S. R. *Chem. Commun.* **2005**, 4789–4791.

(29) Sposato, L. K.; Nettleman, J. H.; LaDuca, R. L. *CrystEngComm* **2010**, *12*, 2374–2380.

(30) Fraser, C. S. A.; Jennings, M. C.; Puddephatt, R. J. *Chem. Commun.* **2001**, 1310–1311.

(31) Arora, K. K.; Pedireddi, V. R. *Cryst. Growth Des.* **2005**, *5*, 1309–1312.

(32) Fan, J.; Sun, W.; Okamura, T.; Zheng, Y.; Sui, B.; Tang, W.; Ueyama, N. *Cryst. Growth Des.* **2004**, *4*, 579–584.

(33) Allendorf, M. D.; Bauer, C. A.; Bhakta, R. K.; Houk, R. T. J. *Chem. Soc. Rev.* **2009**, *38*, 1330–1352 and references therein.